

## Article

# An Innovative Parabolic Trough Collector Design with a Twin-Cavity Receiver

Dimitrios N. Korres <sup>1</sup>, Evangelos Bellos <sup>1,2,\*</sup> , Panagiotis Lykas <sup>1</sup>  and Christos Tzivanidis <sup>1</sup> 

<sup>1</sup> Department of Thermal Engineering, National Technical University of Athens, Zografou, 157 80 Athens, Greece

<sup>2</sup> Department of Mechanical Engineering Educators, School of Pedagogical and Technological Education (ASPETE), 151 22 Amarousion, Greece

\* Correspondence: bellose@central.ntua.gr

**Abstract:** An innovative parabolic trough concentrator coupled to a twin cavity receiver (PTC-TC) in evacuated tube conditions is investigated thermally and optically. The suggested design is compared with a PTC design with a flat receiver (PTC-F) in order to evaluate the efficiency of the proposed configuration. In the very first stages of the study, the optical efficiency was calculated for both collectors, and the optimum design was determined in the PTC-TC case. Then a mass flow rate independency procedure was conducted to ensure accurate results and to make a suitable comparison. The collectors were examined in a wide range of inlet temperatures ranging from 20 °C to 200 °C, and the thermal performance was calculated. Through the comparison process, it was revealed that the proposed collector appears to have higher thermal performance than the typical collector. In particular, there was a mean enhancement of approximately 8%, while the minimum enhancement was found to be greater than 5%. The simulation results regarding both configurations were verified through two models based on theoretical equations. In both geometries, the mean deviations in the verification procedure were lower than 5.6% in both the Darcy friction factor and the Nusselt number. The design and the simulations were conducted with the SolidWorks Flow Simulation tool.

**Keywords:** optical efficiency; thermal efficiency; innovative solar design; PTC; cavity



**Citation:** Korres, D.N.; Bellos, E.; Lykas, P.; Tzivanidis, C. An Innovative Parabolic Trough Collector Design with a Twin-Cavity Receiver. *Appl. Sci.* **2022**, *12*, 12551. <https://doi.org/10.3390/app122412551>

Academic Editors: Diogo Canavarro and Manuel Collares-Pereira

Received: 17 November 2022

Accepted: 5 December 2022

Published: 7 December 2022

**Publisher's Note:** MDPI stays neutral with regard to jurisdictional claims in published maps and institutional affiliations.



**Copyright:** © 2022 by the authors. Licensee MDPI, Basel, Switzerland. This article is an open access article distributed under the terms and conditions of the Creative Commons Attribution (CC BY) license (<https://creativecommons.org/licenses/by/4.0/>).

## 1. Introduction

The parabolic trough collector (PTC) is the best representative of concentrating solar thermal systems and can be utilized in an extended range of applications. A PTC can operate within a wide temperature range, from low temperatures even up to 600 °C, using a large variety of working mediums, from simple water up to sophisticated thermal oils, molten salts, and nanofluids, for ensuring the greatest performance in each individual case. The most well-known areas where a PTC could contribute are electrical power generation, solar cooling (with sorption machines), heating desalination, oil recovery, and dehumidification [1–3].

The vital need for enhancement of PTCs' thermal efficiency has led, over the years, to the development of several different methods and techniques. Typical methods examine the flow regime in the tube, and there has been a great effort to affect and modify positively this regime in order to achieve greater thermal efficiency. This modification happens with the integration of flow inserts as metal fins and foams, as well as twisted tapes and perforated plates, with the use of sophisticated working mediums such as nanofluids and with the use of specially treated tubing systems such as ribbed and corrugated tubes.

Zhu et al. [4] studied the effect of a wavy metal strip on the interior of a PTC tube, and it was revealed that thermal losses were reduced by 18%, which led to greater thermal performance. In another work, Bellos et al. [5] examined a PTC with a novel insert with a star form integrated inside the absorber-flow tube and found that the maximum possible enhancement did not exceed 1%. In the study of Abad et al. [6], copper foam was applied

inside the PTC receiver tube, and this had a significant effect on the convection regime between the receiver and the working medium. In particular, the use of copper foam led to a remarkable enhancement of the Nusselt number, which in turn led to enhanced thermal performance. Moreover, Mwesigye et al. [7] introduced parallel perforated plates at the inner part of the receiver of a PTC in order to improve thermal efficiency. More specifically, the diameter and the distance between the plates, as well as the slope of the latter were optimized, and it was found that the greater the distance between the plates the higher the Reynolds number and thus the intensity of the convective regime. In the study of Liu et al. [8], a twin-twisted tape was inserted in a PTC, and the flow state was examined. It was found that there is an important effect on the formation of the flow from the geometrical characteristics and the orientation of the tapes (swirling direction). Furthermore, Bellos et al. [9] studied a nanofluid-based PTC with wavy configurations at the inner walls of the tube. From the simulation, it came out that in comparison with a typical receiver tube, the thermal performance of the proposed PTC could be slightly enhanced.

Alnaqi et al. [10] examined the effect of a couple of twisted tapes inserted in the absorber of a PTC by using a hybrid nanofluid. In this analysis, various tape diameters and several swirling orientations were tested. It was revealed that the performance of the collector increased when the twin tapes achieved a specific swirling orientation and when the concentration of the nanoparticles in the working medium took higher values. In the study of Rehan et al. [11], the thermal performance of a PTC was set under investigation by applying  $\text{Al}_2\text{O}_3/\text{H}_2\text{O}$  and  $\text{Fe}_2\text{O}_3/\text{H}_2\text{O}$  nanofluids and varying the particle concentrations. It was found that the utilization of nanofluid improves the efficiency of the collector, especially when  $\text{Al}_2\text{O}_3/\text{H}_2\text{O}$  is applied and when the concentration of the nanoparticles increases. As far as the highly concentrating nanofluids, there are many systems that have been examined numerically, and remarkable thermal efficiency enhancements have been observed. However, in real operating conditions, agglomeration issues prevent such an enhancement, and thus the operation of the systems could be affected negatively [12].

Another important aspect, which should be taken into consideration in the PTC thermal efficiency enhancement field, is the design of the receiver and the treatment of its surface. Typical PTC absorbers are usually coated by solar selective materials that ensure significantly high solar absorbance by almost eliminating thermal emissivity. Nevertheless, such coatings are accompanied by special materials and high amounts of energy to be consumed for the production and deposition process. These factors increase remarkably the cost of production and the environmental impact. Hence, it is important to avoid these disadvantages and to find alternative solutions to obtain the desired result. The linear cavity receivers seem to be a novel idea, since they could cooperate with low-cost and environmentally friendly coatings with medium solar absorbance in the range of 0.75 to 0.85 [13,14] by ensuring significantly higher absorbance due to the solar irradiation entrapment [15].

However, only a few studies have been conducted in the field of linear cavity receivers, and most of them are regarding V-cavities [16–24]. For instance, Chen et al. [21] conducted experiments and examined the operation of a novel V-type cavity PTC working with thermal oil. The receiver was insulated with thermal insulation, and the aperture of the receiver was covered by glass. The collector appeared to have a sufficiently high thermal efficiency. The linear circular cavity receiver, which is in the main scope of the present work, has not been examined widely. Korres and Tzivanidis [25] were the first who developed two semi-empirical formulas for estimating the equivalent absorbance of linear circular cavity receivers by taking into consideration the multiple reflections that occur in the cavity. The same research team [15] examined a small PTC with such a cavity receiver enclosed inside an evacuated tube, something that appeared for the first time in the literature. The proposed collector was found to exceed the conventional PTC configuration optically and thermally by 13.0% and 12.2%, respectively. Moreover, in Ref. [26], a PTC with a partially-evacuated cavity receiver was compared with a conventional design, and it was revealed that the cavity design had greater thermal efficiency.

In this work, a new small-scaled PTC with a twin-cavity receiver (PTC-TC) was examined thoroughly and compared with a designed flat receiver PTC (PTC-F). Both designs are novel and are promising solutions, but the twin-cavity idea is a more promising one due to its advanced design. Specifically, the twin-cavity design presents high novelty due to the special design that leads to both high thermal and optical performance, exploiting the advantages of the cavity receivers on a linear concentrating technology. The comparison was conducted regarding thermal and optical efficiency, while the PTC-TC geometry was firstly optimized. In the optimization procedure, several geometrical parameters were taken into account in order to achieve the desired result. Then the two collectors were inserted in the SolidWorks Flow Simulation environment, and two different numerical models were developed. Several different mesh grids were examined in each model in order to ensure independence from the grid results. A similar procedure was performed for the flow rate, and the optimum one was determined for each configuration. Then, the two geometries were compared with each other for a wide range of inlet temperatures from 20 °C up to 200 °C. The thermal efficiency and the thermal losses were determined first. It was revealed that the proposed PTC exceeds the PTC with the flat receiver by 8% on average in thermal performance. Syltherm-800 was used as the working fluid in the collectors, while the latter were designed and simulated in SolidWorks. Moreover, the results arising from the numerical simulation were verified through two different theoretical models. Practically, the objective of the present study was to examine in detail the performance of a twin-cavity receiver and to compare it with another design with a flat absorbing area. The comparison was conducted parametrically, after an initial optimization of some critical design aspects (geometrical and flow) of the twin-cavity receiver.

## 2. Materials and Methods

### 2.1. Examined Configurations

Two PTCs were studied in the present work, one with a twin cavity receiver (PTC-TC) and one with a flat plate absorber (PTC-F). Both receivers were enclosed inside evacuated tubes for ensuring the minimization of thermal losses. The design of the collectors is given in Figure 1. This Figure depicts the geometry of the two examined PTCs. It is important to mention that there is a specific position between the receiver and the reflector in each case. In particular, the receiver with the twin cavities is in a position where the reflector's focal distance is on the centerline axis of it, and all the reflected solar rays end up at the interior of the two cavities. The specific geometry was revealed through an optimization that took place via a ray tracing process in order to ensure the optimum useful power. This optimization is described in the next stages of the manuscript. The positioning in the PTC-F is simpler than in the PTC-TC, since the focal point here is located in the middle of the receiver between the twin tubes. All the models' dimensions are given in Table 1.

**Table 1.** PTC basic dimensions for both designs.

Dimension	PTC-TC	PTC-F
Glass tube outer diameter	56 mm	56 mm
Glass tube thickness	2 mm	2 mm
Receiver outer diameter/width	20 mm	40 mm
Receiver thickness	0.6 mm	0.2 mm
Flow pipe outer diameter	8 mm	8 mm
Flow pipe thickness	0.6 mm	0.6 mm
Focal distance	80 mm	80 mm
Aperture width	200 mm	200 mm
Aperture length	1000 mm	1000 mm

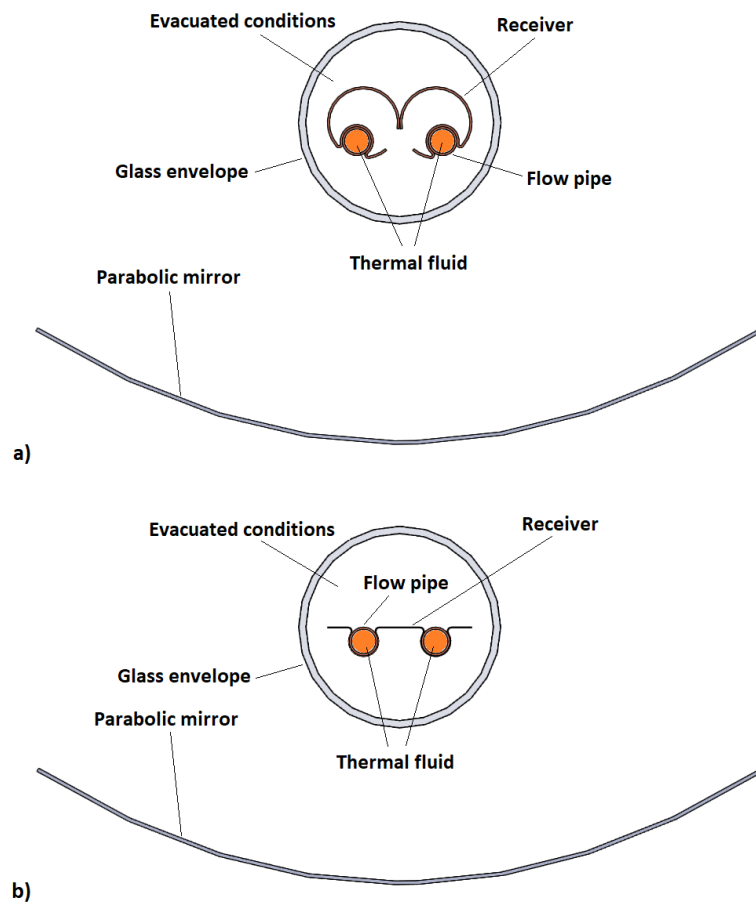


**Figure 1.** The examined designs: (a) PTC-TC, (b) PTC-F.

## 2.2. Operating Conditions and Methodology

### 2.2.1. Ray Tracing

The optical performance was the first parameter that was set under investigation. Ray tracing was done in the SolidWorks Flow Simulation tool, considering the absence of fluid, by taking into account only the absorbed solar power from the receiver in each case. The reflector in each PTC was assumed to have a reflectance ( $\rho$ ) of 94%, while the glass envelope was considered to have 89% transmittance and 88% emittance. The receivers in both PTCs were covered by a coating with a solar absorbance of 80% and a thermal radiation emittance of 10% [13,14]. The available effective solar irradiation in the ray tracing was taken at the value of  $1000 \text{ W/m}^2$ . As for the twin-cavity receiver PTC, an optimization procedure was conducted in order to determine the optimum receiver design. For the particular optimization, three different parameters were put forward, namely,  $\omega$  and  $\phi$  angles, as well as their ( $q$ ) distance, which are depicted in Figure 2.

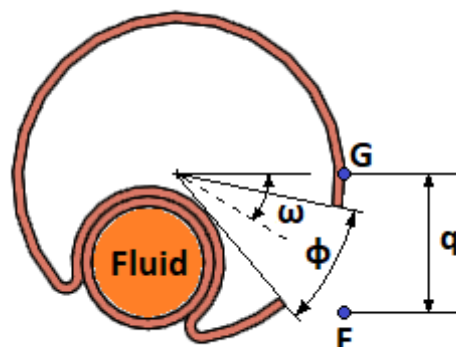


**Figure 2.** Parameters for optical optimization of the PTC-TC.

It is remarkable to state that more than 400 combinations of the optimization parameters were tested for achieving the optimum result. The ( $\omega$ ) and the ( $\varphi$ ) parameters were in the range of  $20^\circ$ – $60^\circ$  and  $20^\circ$ – $100^\circ$ , while the ( $q$ ) distance took values in the range of 2.5 mm up to 25 mm. More specifically, five different values were selected for the ( $\varphi$ ) parameter, eight for the ( $\omega$ ) parameter, and eleven for the ( $q$ ) parameter, with the total combinations reaching the value of 440. Then the optimum geometry was determined, and the optical efficiency was calculated for both examined PTCs.

### 2.2.2. Extensive Simulation

The thermal performance of the two PTCs is a crucial factor, and thus it was examined thoroughly in the present study. In this part, an extensive simulation, including thermal, flow, and optical simulation, was developed and conducted in the SolidWorks Flow Simulation environment for each examined model. The working medium of the analysis was Syltherm-800, and its properties can be found in Ref. [12]. The PTC-F and the PTC-TC were compared to each other as regards the thermal performance and the overall thermal losses. Before the comparison, it was necessary to optimize each model as far as the flow rate is concerned. Hence, several different rates were applied from 40 lt/h up to 480 lt/h, assuming a representative inlet temperature of  $100^\circ\text{C}$ .

A detailed thermal analysis followed the flow rate independency, and the collectors were examined for various inlet temperatures ranging from  $20^\circ\text{C}$  to  $200^\circ\text{C}$ . It should be mentioned that the particular temperature range was within the typical ranges where small-scaled PTCs are being examined [27–29]. The simulations were performed for a flow rate of 160 lt/h, which was determined as the optimum rate for both cases. The direct beam solar irradiation was assumed to be  $1000\text{ W/m}^2$  perpendicular to the aperture, the environment temperature took the value of  $T_a = 20^\circ\text{C}$ , and the wind heat convection coefficient was considered to be  $h_w = 10\text{ W/m}^2/\text{K}$ , which is a typical value. As regards the optical properties of the collectors' subcomponents, these were selected at the same values as in the ray tracing stage.

## 2.3. Simulation Analysis

### 2.3.1. Numerical Simulation Details

The simulation tool for the present work was SolidWorks Flow Simulation [30]. There are many studies where this software has been used in the literature, while various validation/verification procedures have been conducted with experimental results and various theoretical–analytical solutions that make SolidWorks Flow Simulation reliable numerical simulation software [4,7,9,12,15,31–36]. The main assumptions for the simulations are given in Table 2. The third assumption was taken considering that the reflector and the glass envelope were very close to each other, and that the reflector's temperature was close to the ambient temperature. This assumption also appears in several different works [15,36,37]. Another important aspect that should be mentioned is that the thermal simulations were conducted considering a realistic concentration process, and thus the receiver temperature and ray tracing distribution were non-uniform.

**Table 2.** Simulation assumptions.

Assumption Number	Assumption Description
1	Diffusive thermal radiation
2	Grey bodies consideration
3	$T_{\text{sky,eff}} = T_a$
4	Sun shape effect consideration
5	Fully developed flow

### 2.3.2. Sensitivity Analysis

An important step in the development of the simulation models is the mesh independence procedure. Thus, 8 different meshes were examined for every model, aiming to

determine the most suitable one which leads (i) to accurate results and (ii) to a reasonable computational time. The two main criteria were applied for choosing the most suitable mesh for each model, and they were the convergence of the thermal efficiency and of the receiver temperature. Table 3 presents the sensitivity analysis of the mesh independence analysis. The finally selected mesh size had  $1.62 \times 10^6$  elements in the PTC-TC case and  $1.94 \times 10^6$  elements in the PTC-F model. The fluid region was covered by 31% and 26% of the total elements in the PTC-TC and PTC-F, respectively. The mesh was also refined properly on the absorbing surfaces and the solid-to-fluid interfaces. Figure 3 gives the mesh illustration of the interior of the tube in order to present a clear view of the mesh structure. It is important to mention that the fluid mesh was identical in both cases, since the number of fluid cells was  $0.5 \times 10^6$  in both models.

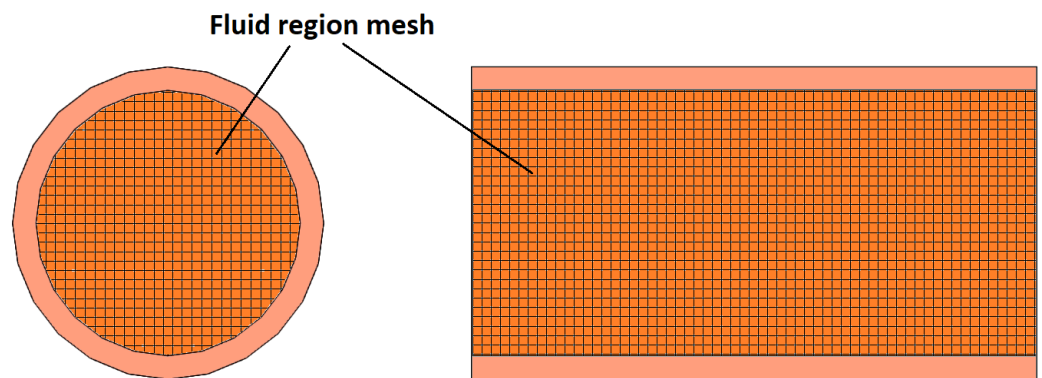


Figure 3. Mesh grid inside the flow tube in both cases.

Table 3. Sensitivity analysis regarding the mesh selection for the PTC-TC and PTC-F.

PTC-TC								
Examined Mesh	1	2	3	4	5	6	7	8
Mesh Cells	$0.49 \times 10^6$	$0.68 \times 10^6$	$0.88 \times 10^6$	$1.11 \times 10^6$	$1.37 \times 10^6$	<b><math>1.62 \times 10^6</math></b>	$1.95 \times 10^6$	$2.25 \times 10^6$
$T_r$ (°C)	109.8	111.5	118.2	118.4	118.6	<b>118.6</b>	118.7	118.7
$\eta_{th}$	74.18%	74.04%	73.44%	73.41%	73.39%	<b>73.37%</b>	73.36%	73.36%
Final selection	Selected mesh							
PTC-F								
Examined Mesh	1	2	3	4	5	6	7	8
Mesh Cells	$0.57 \times 10^6$	$0.75 \times 10^6$	$0.98 \times 10^6$	$1.18 \times 10^6$	$1.39 \times 10^6$	$1.66 \times 10^6$	<b><math>1.94 \times 10^6</math></b>	$2.25 \times 10^6$
$T_r$ (°C)	113.9	115.9	116.2	116.4	116.5	116.5	<b>116.6</b>	116.6
$\eta_{th}$	67.79%	67.70%	67.67%	67.68%	67.66%	67.69%	<b>67.61%</b>	67.63%
Final Selection	Selected mesh							

#### 2.4. Analysis of Equations

In this section, the optical, thermal, and flow analysis equations are provided [38,39]. The thermal efficiency of the PTC is defined as:

$$\eta_{th} = \frac{Q_u}{Q_s} = \frac{Q_u}{A_a \cdot G_{bT}} \tag{1}$$

The optical efficiency of the PTC is defined as:

$$\eta_{opt} = \frac{Q_{abs}}{Q_s} \tag{2}$$

The solar irradiation on the collector surface is calculated as:

$$Q_s = A_a \cdot G_{bT} \quad (3)$$

The useful heat production is calculated as:

$$Q_u = \dot{m} \cdot C_p \cdot (T_o - T_i) = h_f \cdot A_s \cdot (T_s - T_{f,m}) = Q_{abs} - Q_L \quad (4)$$

The mean fluid temperature is estimated as:

$$T_{f,m} = \frac{T_o + T_i}{2} \quad (5)$$

The thermal losses can be calculated as:

$$Q_L = \left[ h_w \cdot (T_g - T_\alpha) + \varepsilon_g \cdot \sigma \cdot (T_g^4 - T_\alpha^4) \right] \cdot A_{g,o} \quad (6)$$

Equation (1) provides two different expressions for thermal efficiency, and Equation (2) indicates that the optical performance is a function of the absorbed solar power ( $Q_{abs}$ ) and the available solar power on the PTC ( $Q_s$ ). The latter is expressed in Equation (3), while the useful output is available in Equation (4). Equation (5) is used for the calculation of the average temperature of the working fluid. Last but not least, the total thermal losses are expressed by Equation (6). Apart from the optical and thermal analysis equations, the respective equations for the flow analysis part are equally significant, and thus it was necessary to present them too [40].

The Reynolds number, which is given in Equation (7), is one of the most important parameters for flow analysis, since it constitutes an indication of the flow regime intensity. The critical Reynolds number in Equation (8) provides us with information on whether or not the flow regime transitions from the laminar to the turbulent [41]. This number is calculated as a function of the Darcy friction factor, which is described in Equation (9) [42]. In Equation (10), the Nusselt number is expressed as the product between the heat convection coefficient inside the flow tube and the inner diameter of the tube divided by the thermal conductivity, which is determined considering the average fluid temperature according to Equation (5). The heat transfer coefficient ( $h_f$ ) is calculated via Equation (4).

$$Re_{D,t} = \frac{u_t \cdot D_{t,i}}{\nu} \quad (7)$$

$$Re_{cr,t} = 140 \cdot \sqrt{8/\lambda_t} \quad (8)$$

$$\lambda_t = 2 \cdot \frac{D_{t,i}}{L_t} \cdot \frac{\Delta p_t}{u_t^2 \cdot \rho_f} \quad (9)$$

$$Nu = \frac{h_f \cdot D_{t,i}}{k_f} \quad (10)$$

Regarding the verification procedure, Equations (11)–(14) were applied. These equations represent the theoretical expressions of the Nusselt number and the Darcy friction factor for the laminar (Equations (11) and (13)) and the turbulent (Equations (12) and (14)) conditions, respectively [12,15,42–44]. Equations (11) and (13) are applied for the verification of the numerical models when the critical values of the Reynolds number are less than the unit. In the cases where the critical Reynolds number becomes greater than 1, Equations (12) and (14) are put forward for the verification process.

$$\lambda_{t,lam} = \frac{64}{Re_{D,t}} \quad (11)$$

$$\lambda_{t,tur} = 0.25 \cdot \left( \log \left( 7 / \left( Re_{D_{1,i}} \right)^{0.9} \right) \right)^{-2} \quad (12)$$

$$Nu_{lam} = \frac{3.66 + 0.0668 \cdot Re_{D_i} \cdot Pr \cdot D_t / L_t}{\left( 1 + 0.04 \cdot \left( Re_{D_i} \cdot Pr \cdot D_t / L_t \right)^{2/3} \right)} \quad (13)$$

$$Nu_{tur} = 0.023 \cdot Re_{D_{1,i}}^{0.8} \cdot Pr^{0.4} \quad (14)$$

### 3. Results and Discussion

#### 3.1. Verification of the Developed Models

Before proceeding with the optical and thermal analysis results, it is essential to present the verification results regarding the two numerical models that were developed in the present work. The verification was conducted for the whole operating temperature range using two different models from theory (see Equations (11)–(14)) as concerns the Darcy friction factor as well as the Nusselt number. To use the abovementioned formulas properly, it was necessary to define when the flow transition from the laminar to the turbulent regime took place in every PTC. It could be found by calculating the Reynolds ratio ( $Re/Re_{cr}$ ), as Figure 4 suggests.

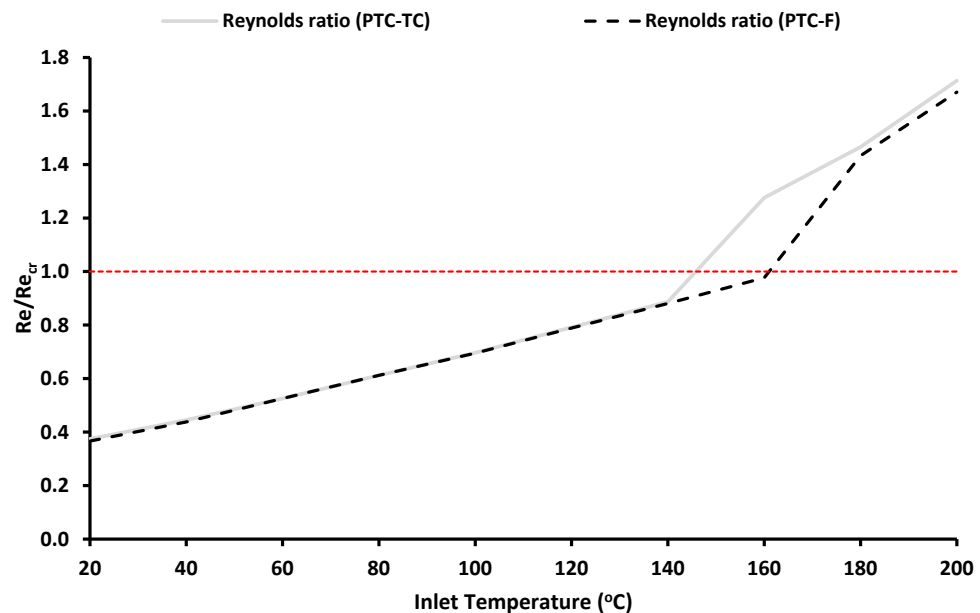


Figure 4. Reynolds ratio for both PTCs (the horizontal dotted red line indicates the transition limit).

As is depicted in Figure 4, the transition to the turbulent state was different for each PTC. More specifically, the transition happened from 140 °C to 160 °C in the PTC-TC and in the range of 160 °C to 180 °C in the PTC-F. This difference existed due to the higher temperature levels of the PTC-TC against the PTC-F. Hence, the theoretical models were applied for the whole operating temperature range by also taking into consideration the transition regions, which came from Figure 4. Figure 5 presents the verification results concerning the Nusselt number and the Darcy friction factor for the PTC-TC. The respective results for the PTC-F are given in Figure 6.

Figures 5 and 6 show that there is an acceptable agreement between the CFD and the theoretical results. In particular, the mean declination from the theoretical values does not exceed 5.0% as regards the PTC-TC in the Nusselt number and the Darcy friction factor. As far as the PTC-F is concerned, this declination is lower than 5.6%. Moreover, Figures 5 and 6 indicate the transition from the laminar flow regime to the turbulent flow regime. It is clear that the transition regions are identical to those found in Figure 4 from the Reynolds ratio calculation.

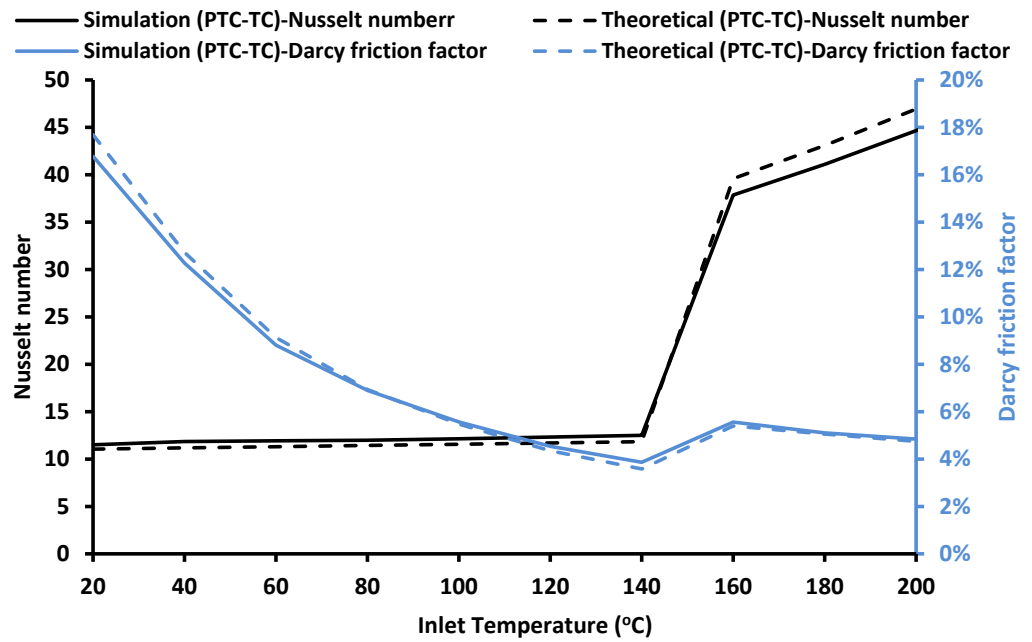


Figure 5. Verification evidence for the PTC-TC design regarding the flow and heat transfer.

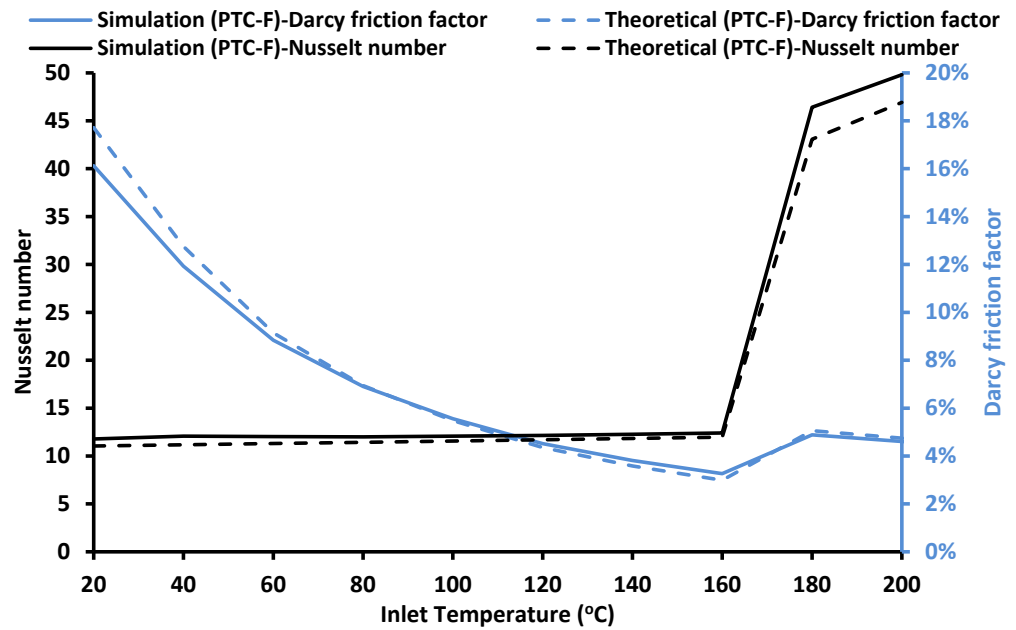
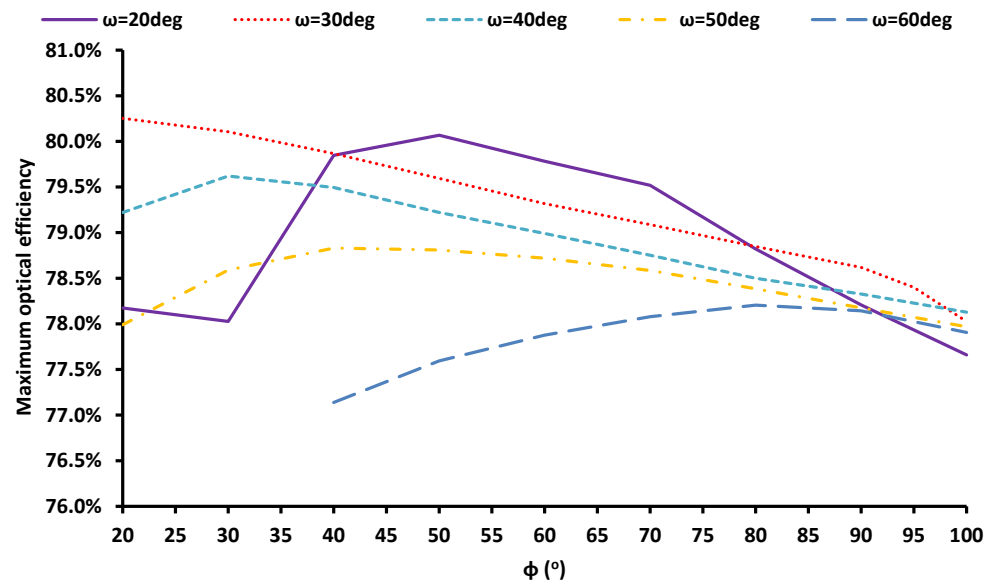


Figure 6. Verification evidence for the PTC-F design regarding the flow and heat transfer.

### 3.2. Optical Analysis Results

This subsection refers to the results coming from the optical optimization of the PTC-TC as far as the geometry of the cavities is concerned. The optimization was based on three different parameters ( $\omega$ ,  $\varphi$ , and  $q$ ), while several different combinations were examined for achieving the desired result. The optimization results are presented in Figure 7. More specifically, the specific chart depicts five different efficiency curves, each one of which corresponds to a specific ( $\omega$ ) value as a function of the ( $\varphi$ ) parameter. These curves were plotted considering the ( $q$ ) values that ensure the maximum optical performance in each case.



**Figure 7.** PTC-TC optimization results: optical efficiency values for different combinations of the parameters ( $\varphi$ ) and ( $\omega$ ).

Figure 7 shows that the optical performance declines with the increment of the cavity angular aperture ( $\varphi$ ). This happens because the lower the ( $\varphi$ ) parameter, the higher the solar radiation entrapment and vice versa. Moreover, the optical performance shows the same behavior as the ( $\omega$ ) parameter also increases. Thus, according to Figure 7, the best solution seems to be a twin cavity with  $\omega = 30^\circ$  and  $\varphi = 20^\circ$ . However, a more detailed analysis revealed that in this case as well as in the scenario where  $\varphi = 30^\circ$ , the maximization of the optical performance was observed for only a specific ( $q$ ) value, and thus there was not any sustainability. The same also happened in the case where  $\omega = 20^\circ$ . For these reasons, a ( $\varphi$ ) of  $40^\circ$  was finally selected with  $\omega = 30^\circ$  and  $q = 8$  mm. This configuration showed an optical performance of 79.9%. As regards the PTC-F optical performance, the ray tracing results indicated an optical performance of 72.52%. In other words, the PTC-TC configuration seemed to exceed significantly the PTC-F in optical performance, providing an enhancement of 10.14%, which is remarkable.

### 3.3. Thermal Analysis Results

This section is dedicated to the results concerning the thermal investigation of the studied collectors. The thermal efficiency and the total thermal losses are presented in Figures 8 and 9, respectively, for the whole operating range ( $20^\circ\text{C}$ – $200^\circ\text{C}$ ) of this study. Figure 8 comes to prove the superiority of the PTC-TC against the PTC-F in thermal efficiency. More particularly, the mean enhancement gained from the use of the cavity configuration reached 8%, which is a remarkable percentage for this kind of application. The specific enhancement ranged from 5.25% up to 9.85%, achieving its lower values in high operating temperatures due to the increase of heat losses. According to Figure 9, thermal losses seemed to take reasonably higher values in the PTC-TC geometry, since the receiver surface in the latter was much greater than in the PTC-F.

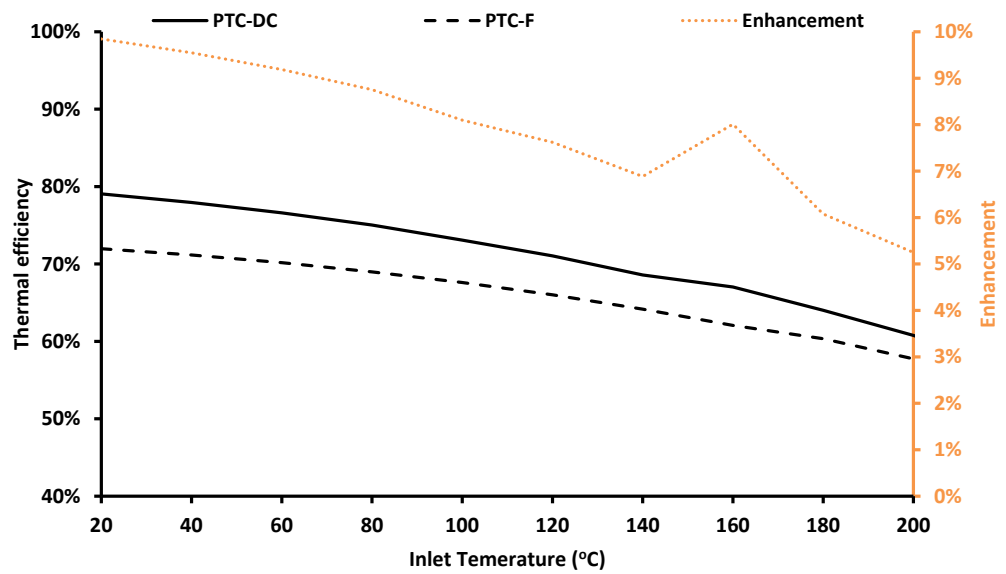


Figure 8. Thermal efficiency of the PTC-TC and PTC-F.

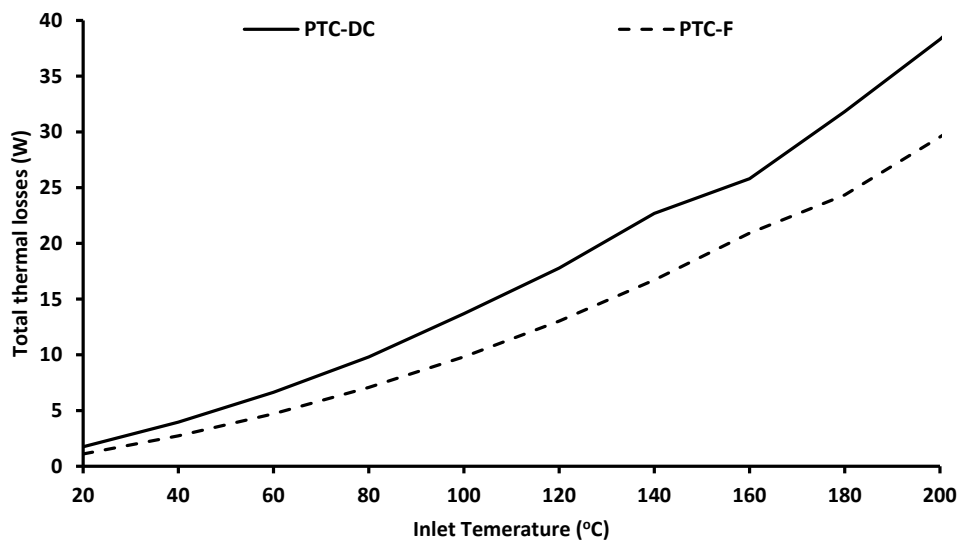


Figure 9. Total thermal losses of the PTC-TC and PTC-F.

In Figures 10 and 11, the mean values of the receiver and the glass temperature are presented for the whole operating range. As Figure 10 shows, the receiver temperature seemed to be greater in the PTC-TC case for almost the whole operating range. This is reasonable considering that the receiver of the PTC-TC absorbed 10.14% more solar irradiation than the PTC-F receiver. It is interesting to comment that for the inlet temperature of around 160 °C, the temperature of the receiver for the PTC-F was about 7 K higher compared to the PTC-TC case. This result happened due to the earlier transition of the PTC-TC to the turbulent state compared to the PTC-F. According to Figure 11, the glass temperature level was higher in the PTC-TC, which is a reasonable result because the receiver absorbed more solar power and it also had a greater size than that of the PTC-F geometry.

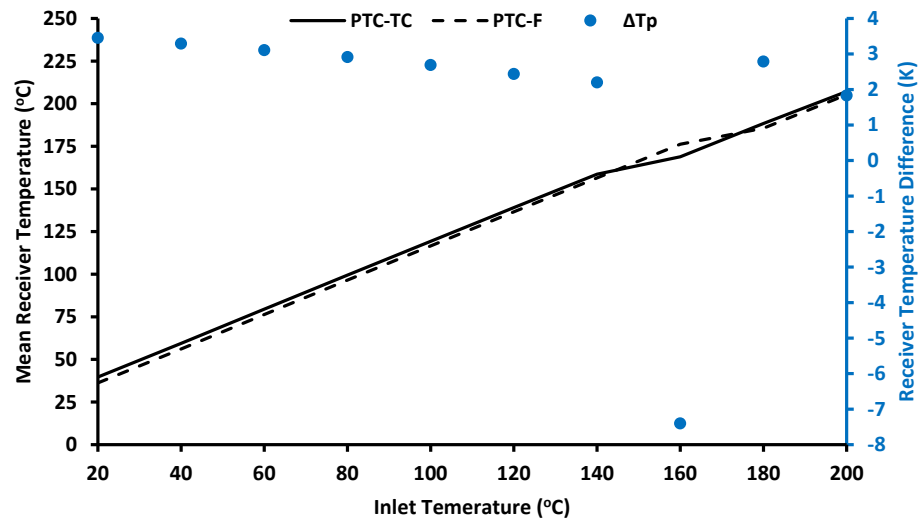


Figure 10. Mean receiver temperature comparison.

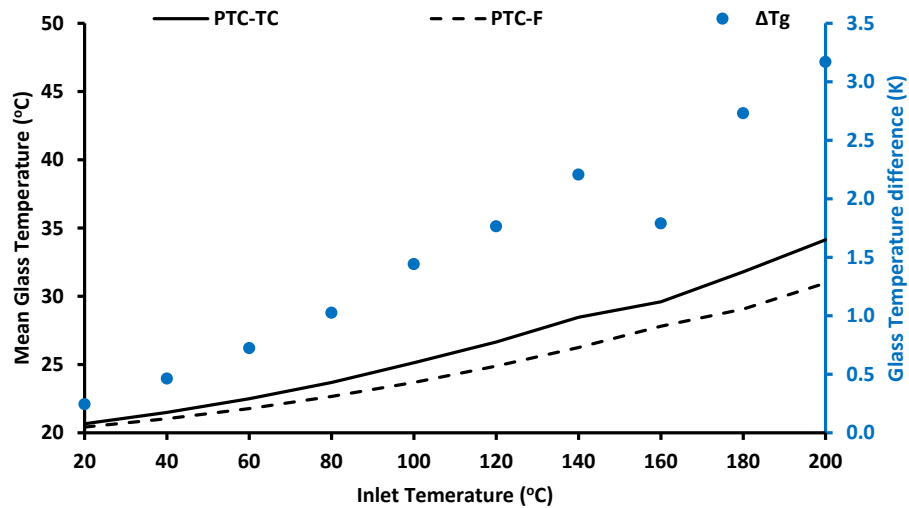


Figure 11. Mean glass temperature comparison.

Figure 12 illustrates the receiver temperature allocation for the operating point of  $T_i = 100\text{ }^\circ\text{C}$  for each PTC. As Figure 12 shows, the receiver temperature fields were higher in the PTC-TC scenario than expected, since in this case, the solar absorption was greater. It is also critical to say that the temperature in both receivers had, reasonably, higher values in the region where the solar irradiation was concentrated in every case. This proves that the ray tracing simulation is very close to the real ray tracing procedure.

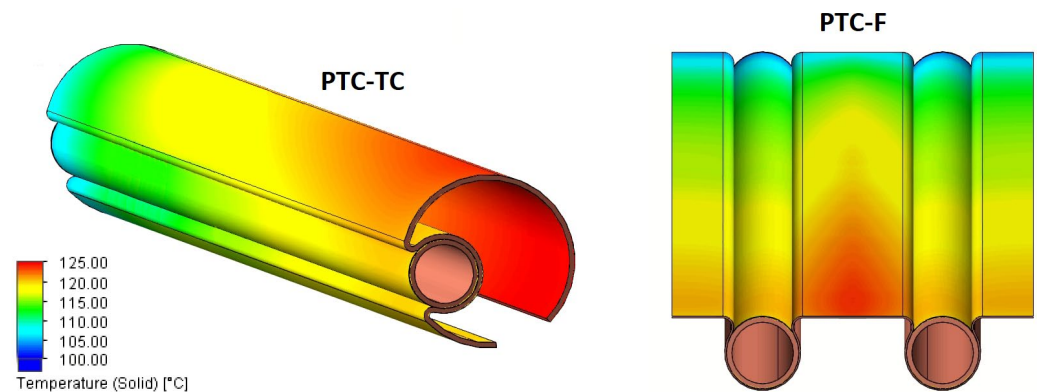
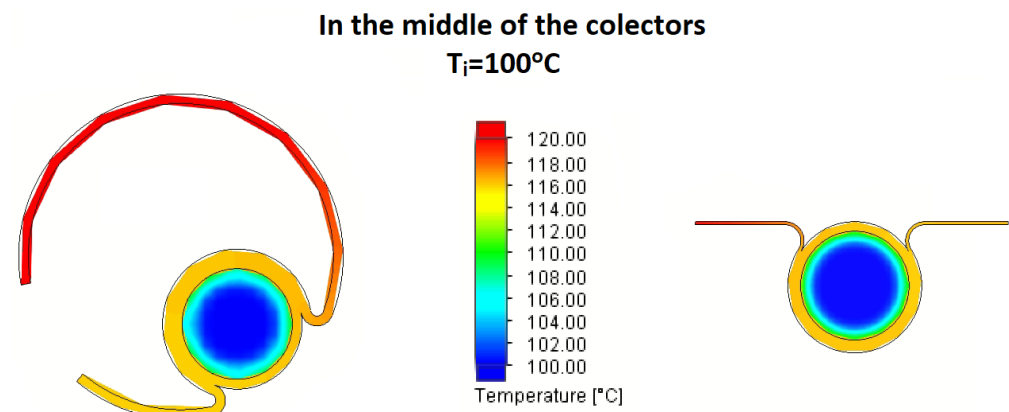
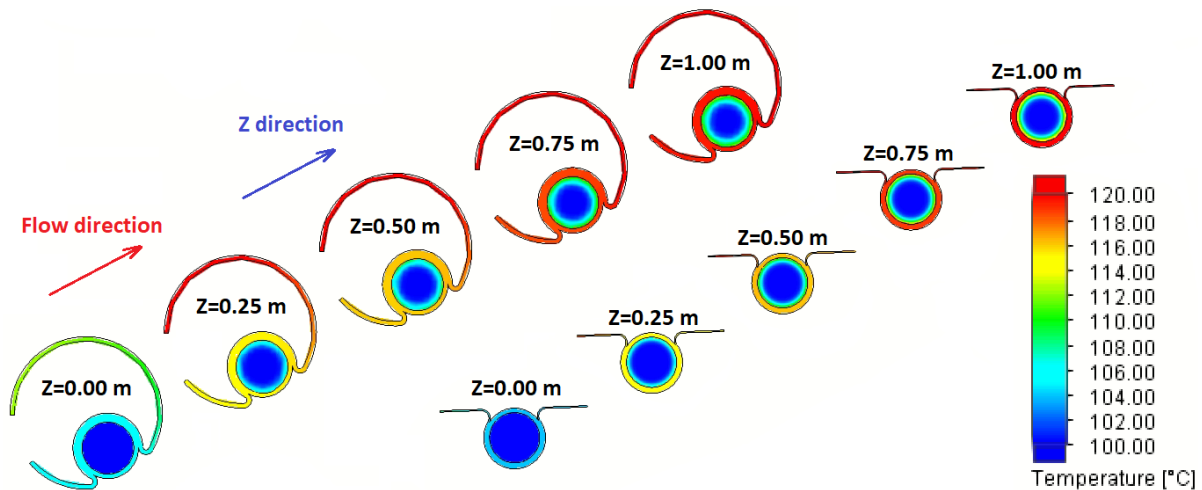


Figure 12. Receiver temperature allocation for an inlet temperature at  $100\text{ }^\circ\text{C}$ .

Figure 13 gives an illustration of the temperature fields of the working medium and the receiver at a transversal section of both collectors in the middle of them. It is clear, as seen in Figure 13, that the temperature of the working fluid was higher in the cavity receiver case, as was expected. The same happened with the temperature of solid bodies. Both occurred because the receiver in the cavity case was greater, and it absorbed more solar irradiation with a much greater equivalent solar absorbance. Figure 14 depicts the temperature distribution in the receiver and the working fluid in each collector through several transversal sections along each absorber. It became obvious that the temperature allocations were becoming higher going from the inlet to the outlet of the collectors. In addition, the PTC-TC seemed to prevail against the PTC-F, appearing in higher temperature fields in all the compared positions along the collectors.



**Figure 13.** Temperature allocations of the receiver and the working fluid in the middle of the collectors for an inlet temperature of 100 °C.



**Figure 14.** Temperature allocations of the receiver and the working fluid in several different sections along the collectors for an inlet temperature of 100 °C.

At this point, it is useful to discuss the findings of the present work. It is clear that both examined designs were efficient choices for operation up to 200 °C. The PTC with the twin-cavity was the best choice, and this fact indicates that the use of the twin-cavity is a promising choice for the design of future PTCs that operate at medium temperatures. Generally, the results of the present work indicate thermal efficiency of over 60% which is a very promising result concerning the system viability. The advantage of the suggested design is the lower cost compared to the conventional PTC due to the lack of the evacuated tube which is an expensive component of the PTC.

In the future, it is important to test the present solar system coupled to applications (e.g., solar cooling or power production with organic Rankine cycle) in order to evaluate the

systems energetically and economically. Moreover, the present systems can be examined for different solar angles in order to determine their optical performance for different operating conditions, and so it will be possible to examine these systems on a daily basis. Last but not least, the experimental investigation of the suggested configurations is a critical next step that has to be conducted for extracting extra conclusions regarding their operation.

#### 4. Conclusions

In this work, a new type of PTC with a twin-cavity receiver is introduced as an alternative solution for small-scaled PTC applications. The investigation was conducted for a typical operating temperature range of such applications, which extends from 20 °C up to 200 °C. The specific collector was also compared to a PTC with a flat plate absorber configuration.

First of all, it is important to mention that the simulation results were verified through their respective theoretical results. In the verification process, there was excellent agreement between the theoretical and the CFD results, with the mean deviations being lower than 5.6% in both cases. This fact ensures the reliability of the present simulations. Moreover, it is significant to mention the superiority of the PTC-TC versus the PTC-F in optical and thermal terms. Particularly, there is a great enhancement of 10.14% in optical efficiency, while the respective improvement in thermal efficiency reaches 9.85% in low temperatures and 5.25% in high ones.

As a general conclusion, it must be noted that the proposed collector (PTC-TC) was optimized and found to far exceed the PTC with the flat receiver (PTC-F) in optical and thermal performance. This fact indicates the superiority of the suggested geometry and its potential for being applied as an alternative solution in small-scaled PTC applications. Generally, the results indicate that the thermal efficiency of the PTC-TC is over 60%, which is a very promising result concerning the system's viability.

**Author Contributions:** Methodology, D.N.K., E.B. and P.L.; Software, D.N.K.; Validation, D.N.K.; Formal analysis, D.N.K.; Investigation, D.N.K., E.B. and P.L.; Writing—original draft, D.N.K., E.B., P.L. and C.T.; Supervision, E.B. and C.T. All authors have read and agreed to the published version of the manuscript.

**Funding:** This research was funded by Bodossaki Foundation.

**Institutional Review Board Statement:** Not applicable.

**Informed Consent Statement:** Not applicable.

**Data Availability Statement:** Data available after request.

**Acknowledgments:** The first author would like to thank the Bodossaki Foundation for its financial support in his post-doctoral research.

**Conflicts of Interest:** The authors declare no conflict of interest.

#### Nomenclature

A	Area, m <sup>2</sup>
C <sub>p</sub>	Specific heat capacity, kJ/(kgK)
D	Diameter, m
G	Solar irradiation, W/m <sup>2</sup>
h	Heat convection coefficient, W/(m <sup>2</sup> K)
k	Thermal conductivity, W/(mK)
L	Length, m
m	Mass flow rate, kg/s
Nu	Nusselt number
p	Pressure level, N/m <sup>2</sup>
Pr	Prandtl number
Q	Heat rate, W

q	Distance between “F” and “G” points, m
Re	Reynolds number
T	Temperature level, °C
u	Fluid speed, m/s
w	Width, m
<b>Greek symbols</b>	
$\alpha$	Absorbance
$\epsilon$	Emittance
$\eta$	Efficiency
$\lambda$	Darcy friction factor
$\nu$	Kinematic viscosity, m <sup>2</sup> /s
$\rho$	Density, kg/m <sup>3</sup> , or Reflectance
$\sigma$	Boltzmann constant, W/(m <sup>2</sup> K <sup>4</sup> )
$\tau$	Transmittance
$\varphi$	Angular aperture of the cavity, °
$\omega$	Rotation angle of the cavity, °
<b>Abbreviations</b>	
PTC	Parabolic trough collector
PTC-TC	PTC with twin-cavity receiver
PTC-F	PTC with flat receiver
<b>Subscripts</b>	
$\alpha$	Ambient or Aperture
abs	Absorbed
cr	Critical
bT	Direct beam
f	Working fluid
g	Glass
i	Inlet “for T” or “for D”
L	Overall thermal losses
lam	Laminar
m	Mean
o	Outlet “for T” or “for A”
opt	Optical
p	Absorber
R	Reflector
s	Solar or Tube’s wall
t	Flow tube
th	Thermal
u	Useful
w	Wind

## References

1. Najafi, A.; Jafarian, A.; Arabkoohsar, A. A thorough three-dimensional simulation of steam generating solar parabolic trough collectors, a benchmark of various methods’ accuracy. *Sustain. Energy Technol. Assess.* **2021**, *47*, 101456. [\[CrossRef\]](#)
2. Arnaoutakis, N.; Milousi, M.; Papaefthimiou, S.; Fokaides, P.A.; Caouris, Y.G.; Souliotis, M. Life cycle as-sessment as a methodological tool for the optimum design of integrated collector storage solar water heaters. *Energy* **2019**, *182*, 1084–1099. [\[CrossRef\]](#)
3. Bellos, E.; Tzivanidis, C. Alternative designs of parabolic trough solar collectors. *Prog. Energy Combust. Sci.* **2019**, *71*, 81–117. [\[CrossRef\]](#)
4. Zhu, X.; Zhu, L.; Zhao, J. Wavy-tape insert designed for managing highly concentrated solar energy on absorber tube of parabolic trough receiver. *Energy* **2017**, *141*, 1146–1155. [\[CrossRef\]](#)
5. Bellos, E.; Tzivanidis, C. Investigation of a star flow insert in a parabolic trough solar collector. *Appl. Energy* **2018**, *224*, 86–102. [\[CrossRef\]](#)
6. Jamal-Abad, M.T.; Saedodin, S.; Aminy, M. Experimental investigation on a solar parabolic trough collector for absorber tube filled with porous media. *Renew. Energy* **2017**, *107*, 156–163. [\[CrossRef\]](#)
7. Mwesigye, A.; Bello-Ochende, T.; Meyer, J.P. Multi-objective and thermodynamic optimisation of a parabolic trough receiver with perforated plate inserts. *Appl. Therm. Eng.* **2015**, *77*, 42–56. [\[CrossRef\]](#)
8. Liu, Y.; Chen, Q.; Hu, K.; Hao, J.-H. Flow field optimization for the solar parabolic trough receivers in direct steam generation systems by the variational principle. *Int. J. Heat Mass Transf.* **2016**, *102*, 1073–1081. [\[CrossRef\]](#)

9. Bellos, E.; Tzivanidis, C.; Antonopoulos, K.; Gkinis, G. Thermal enhancement of solar parabolic trough collectors by using nanofluids and converging-diverging absorber tube. *Renew. Energy* **2016**, *94*, 213–222. [[CrossRef](#)]
10. Alnaqi, A.A.; Alsarraf, J.; Al-Rashed, A. Hydrothermal effects of using two twisted tape inserts in a parabolic trough solar collector filled with MgO-MWCNT/thermal oil hybrid nanofluid. *Sustain. Energy Technol. Assess.* **2021**, *47*, 101331.
11. Rehan, M.A.; Ali, M.; Sheikh, N.A.; Khalil, M.S. Experimental performance analysis of low concentration ratio solar parabolic trough collectors with nanofluids in winter conditions. *Renew. Energy* **2018**, *118*, 742–751. [[CrossRef](#)]
12. Korres, D.; Bellos, E.; Tzivanidis, C. Investigation of a nanofluid-based compound parabolic trough solar collector under laminar flow conditions. *Appl. Ther. Eng.* **2018**, *149*, 366–376. [[CrossRef](#)]
13. Zhang, X.; Wang, X.; Zhang, X.; Li, Y.; Cheng, X. Effect of multilayered CoO-CoAl<sub>2</sub>O<sub>4</sub> films on improving solar absorptance of Co-WC solar selective absorbing coatings. *Vacuum* **2018**, *155*, 185–192. [[CrossRef](#)]
14. Katumba, G.; Lu, J.; Olumekor, L.; Westin, G.; Wäckelgard, E. Low Cost Selective Solar Coatings: Characteristics of Carbon-In-Silica Synthesized with Sol-Gel Technique. *J. Sol-Gel Sci. Technol.* **2005**, *36*, 33–43. [[CrossRef](#)]
15. Korres, D.N.; Tzivanidis, C. Investigation of a novel small-sized bifacial cavity PTC and comparison with conventional configurations. *Ther. Sci. Eng. Prog.* **2019**, *17*, 100355. [[CrossRef](#)]
16. Ardeh, E.A.; Loni, R.; Najafi, G.; Ghobadian, B.; Bellos, E.; Wen, D. Exergy and economic assessments of solar organic Rankine cycle system with linear V-Shape cavity. *Energy Convers. Manag.* **2019**, *199*, 111997. [[CrossRef](#)]
17. Loni, R.; Ghobadian, B.; Kasaeian, A.B.; Akhlaghi, M.M.; Bellos, E.; Najafi, G. Sensitivity analysis of parabolic trough concentrator using rectangular cavity receiver. *Appl. Therm. Eng.* **2020**, *169*, 114948. [[CrossRef](#)]
18. Lin, M.; Sumathy, K.; Dai, Y.; Wang, R.; Chen, Y. Experimental and theoretical analysis on a linear Fresnel reflector solar collector prototype with V-shaped cavity receiver. *Appl. Eng.* **2013**, *51*, 963–972. [[CrossRef](#)]
19. Zhang, L.; Fang, J.; Wei, J.; Yang, G. Numerical investigation on the thermal performance of molten salt cavity receivers with different structures. *Appl. Energy* **2017**, *204*, 966–978. [[CrossRef](#)]
20. Pavlovic, S.; Daabo, A.M.; Bellos, E.; Stefanovic, V.; Mahmoud, S.; Al-Dadah, R.K. Experimental and Numerical Investigation on the Optical and Thermal Performance of Solar Parabolic Dish and Corrugated Spiral Cavity Receiver. *J. Clean. Prod.* **2017**, *150*, 75–92. [[CrossRef](#)]
21. Chen, F.; Li, M.; Zhang, P.; Luo, X. Thermal performance of a novel linear cavity absorber for parabolic trough solar concentrator. *Energy Convers. Manag.* **2014**, *90*, 292–299. [[CrossRef](#)]
22. Xiao, X.; Zhang, P.; Shao, D.; Li, M. Experimental and numerical heat transfer analysis of a V-cavity absorber for linear parabolic trough solar collector. *Energy Convers. Manag.* **2014**, *86*, 49–59. [[CrossRef](#)]
23. Liang, H.; Fan, M.; You, S.; Xia, J.; Zhang, H.; Wang, Y. An analysis of the heat loss and overheating protection of a cavity receiver with a novel movable cover for parabolic trough solar collectors. *Energy* **2018**, *158*, 719–729. [[CrossRef](#)]
24. Al-Nimr, M.; Al-Darawsheh, I.; Al-Khalayleh, L. A novel hybrid cavity solar thermal collector. *Renew. Energy* **2018**, *115*, 299–307. [[CrossRef](#)]
25. Korres, D.N.; Tzivanidis, C. Development of two new semi-empirical formulas for estimation of solar absorptance in circular cavity receivers. *Therm. Sci. Eng. Prog.* **2019**, *10*, 147–153. [[CrossRef](#)]
26. Avargani, V.M.; Norton, B.; Rahimi, A. An open-aperture partially-evacuated receiver for more uniform reflected solar flux in circular-trough reflectors: Comparative performance in air heating applications. *Renew. Energy* **2021**, *176*, 11–24. [[CrossRef](#)]
27. Fernández-García, A.; Valenzuela, L.; Zarza, E.; Rojas, E.; Pérez, M.; Hernández-Escobedo, Q.; Manzano-Agugliaro, F. SMALL-SIZED parabolic-trough solar collectors: Development of a test loop and evaluation of testing conditions. *Energy* **2018**, *152*, 401–415. [[CrossRef](#)]
28. Lobón, D.H.; Valenzuela, L. Impact of pressure losses in small-sized parabolic-trough collectors for direct steam generation. *Energy* **2013**, *61*, 502–512. [[CrossRef](#)]
29. Zou, B.; Dong, J.; Yao, Y.; Jiang, Y. An experimental investigation on a small-sized parabolic trough solar collector for water heating in cold areas. *Appl. Energy* **2016**, *163*, 396–407. [[CrossRef](#)]
30. *Technical Reference Solidworks Flow Simulation 2015*, Dassault Systems, 2015.
31. Korres, D.N.; Tzivanidis, C. Simulation and Optimization of a Mini Compound Parabolic Collector with a Coaxial Flow System. In *The Role of Exergy in Energy and the Environment. Green Energy and Technology*; Springer: Cham, Switzerland, 2018; Chapter 47, pp. 663–675. [[CrossRef](#)]
32. Korres, D.N.; Tzivanidis, C.; Koronaki, I.P.; Nitsas, M.T. Experimental, numerical and analytical investigation of a U-type evacuated tube collectors' array. *Renew. Energy* **2019**, *135*, 218–231. [[CrossRef](#)]
33. Korres, D.N.; Tzivanidis, C. Numerical investigation and optimization of an experimentally analyzed solar CPC. *Energy* **2019**, *172*, 57–67. [[CrossRef](#)]
34. Pavlovic, S.; Loni, R.; Bellos, E.; Vasiljević, D.; Najafi, G.; Kasaeian, A. Comparative study of spiral and conical cavity receivers for a solar dish collector. *Energy Convers. Manag.* **2018**, *178*, 111–122. [[CrossRef](#)]
35. Korres, D.N.; Tzivanidis, C. A symmetric and an asymmetric mini Compound Parabolic Collector under Optical Investigation. In *The Role of Exergy in Energy and the Environment: Green Energy and Technology*; Springer: Cham, Switzerland, 2018; Chapter 46; pp. 649–661. [[CrossRef](#)]
36. Korres, D.; Tzivanidis, C. A new mini-CPC under thermal and optical investigation. *Renew. Energy* **2018**, *128*, 529–540. [[CrossRef](#)]

37. Ataee, S.; Ameri, M. Energy and exergy analysis of all-glass evacuated solar collector tubes with coaxial fluid conduit. *Sol. Energy* **2015**, *118*, 575–591. [[CrossRef](#)]
38. Duffie, J.; Beckmann, W. *Solar Engineering of Thermal Processes*, 4th ed.; John Wiley & Sons Inc.: New York, NY, USA, 2013.
39. Korres, D.N.; Bellos, E.; Tzivanidis, C. Integration of a Linear Cavity Receiver in an Asymmetric Compound Parabolic Collector. *Energies* **2022**, *15*, 8635. [[CrossRef](#)]
40. Leinhard, J., IV; Leinhard, V.J. *A Heat Transfer Textbook*, 4th ed.; Philogiston Press: Cambridge, MA, USA, 2012; p. 577.
41. Ohm, M.; Iguchi, M. Critical Reynolds Number in an Oscillating Pipe Flow. *Bull. Jsme* **1982**, *25*, 165–172. [[CrossRef](#)]
42. Bergman, T.L.; Lavine, A.S.; Incropera, F.P.; Dewitt, D.P. *Fundamentals of Heat and Mass Transfer*, 7th ed.; John Wiley & Sons: New York, NY, USA, 2011.
43. Taler, D. Determining velocity and friction factor for turbulent flow in smooth tubes. *Int. J. Ther. Sci.* **2016**, *105*, 109–122. [[CrossRef](#)]
44. Fang, X.; Zhou, Y.X.Z. New correlations of single-phase friction factor for turbulent pipe flow and evaluation of existing single-phase friction factor correlations. *Nucl. Eng. Des.* **2011**, *241*, 897–902. [[CrossRef](#)]